

JPET #114496

Title page

Local inhibition of liver fibrosis by specific delivery of a PDGF kinase inhibitor to hepatic stellate cells

Teresa Gonzalo¹, Leonie Beljaars, Marja van de Bovenkamp, Kai Temming, Anne-Miek van Loenen, Catharina Reker-Smit, Dirk K.F. Meijer, Marie Lacombe, Frank Opdam, György Kéri, László Örfi, Klaas Poelstra, Robbert J. Kok.

Department of Pharmacokinetics and Drug Delivery, Groningen University Institute for Drug Exploration, University of Groningen, The Netherlands (T.G., L.B, M.B., K.T., A.L., C.R-S., D.K.F.M., K.P., R.J.K.).

Kreatech Biotechnology B.V., Amsterdam, The Netherlands (K.T., M.L., F.O.).

Departments of Medical and Pharmaceutical Chemistry, Semmelweis University, Budapest, Hungary (G.K., L.O.)

Department of Pharmaceutics, Utrecht Institute for Pharmaceutical Sciences, The Netherlands (R.J.K.).

JPET #114496

Running title page

Running title

Antifibrotic effects of an HSC-directed kinase inhibitor

Corresponding author:

Robbert J. Kok, PhD

Department of Pharmaceutics, Utrecht Institute for Pharmaceutical Sciences (UIPS),

Sorbonnelaan 16, 3584 CA Utrecht, The Netherlands

Phone: +31-30-2534724

Fax: +31-30-2517839

Email: r.j.kok@pharm.uu.nl

document statistics:

Number of text pages: 35

Number of tables: 2

Number of figures: 8

Number of references: 39

Number of words in Abstract: 244

Number of words in Introduction: 632

Number of words in Discussion: 1555

Abbreviations:

HSC, hepatic stellate cells; PDGF, Platelet Derived Growth Factor; M6PHSA, mannose 6-phosphate modified human serum albumin; PAP19, phenyl-amino-pyrimidine derivative 19; ULS, Universal Linkage System; α SMA, α -smooth muscle actin; BDL, bile duct ligated; M6P/IGFII, mannose-6-phosphate/Insulin-like growth factor-II; DMF, dimethylformamide; ALT, alanine amino transferase; AP, alkaline phosphatase; Glyceraldehyde-3-phosphate dehydrogenase, GAPDH; TIMP-1, Tissue Inhibitor of Metalloproteinases-1; HSA, human serum albumin.

Recommended section:

Gastrointestinal, Hepatic, Pulmonary and Renal

JPET #114496

Abstract

Liver fibrosis is characterized by excessive proliferation and activation of hepatic stellate Cells (HSC), a process in which platelet-derived growth factor (PDGF) plays an important role. Inhibition of liver fibrosis via specific delivery of a PDGF kinase inhibitor to HSC might therefore be an attractive strategy. The HSC-selective carrier M6PHSA (mannose-6-phosphate modified human serum albumin) was equipped with a tyrosine kinase inhibitor (PAP19, an imatinib derivative) by means of the platinum-based universal linkage system (ULS). The antifibrotic activity of PAP19-M6PHSA was evaluated in culture-activated rat HSC and precision-cut liver slices from fibrotic rats. After 24h incubation, both free inhibitor PAP19 and PAP19-M6PHSA showed potent activity, as determined by quantitative RT-PCR analysis of α -smooth muscle actin (α SMA) and procollagen 1a1. Next, we examined the organ distribution and antifibrotic activity of PAP19-M6PHSA in bile duct ligated (BDL) rats. Male Wistar rats at day 10 after BDL were administered a single dose of PAP19-M6PHSA and sacrificed at 2h, 1 day or 2 days afterwards. The accumulation of PAP19-M6PHSA in the liver was quantified by HPLC analysis (30% of the injected dose at 2h) and detected in the liver by staining of the carrier. Liver drug levels were sustained at 24h and 48h after the single dose. Furthermore, PAP19-M6PHSA reduced collagen deposition (sirius-red staining) and α SMA staining of activated HSC at these time points in comparison with saline-treated rats. We therefore conclude that delivery of a PDGF-kinase inhibitor to HSC is a promising technology to attenuate liver fibrogenesis.

JPET #114496

Introduction

Liver fibrosis is a proliferative disease that may be initiated by a variety of factors including chronic hepatitis, virus infections, alcohol drinking, and drug abuse. It has been extensively documented that activated hepatic stellate cells (HSC) play a fundamental role in the development of liver fibrosis (Friedman, 1999; Tsukada et al., 2006). During liver fibrosis, activated HSC proliferate and deposit extracellular matrix proteins, a process that is driven by an array of cytokines and growth factors. Among these, platelet-derived growth factor has been identified as the most potent mitogen for HSC (Pinzani, 2002). Activated HSC produce PDGF (Wong et al., 1994) and PDGFR- β receptors are highly upregulated on the cell surface of hepatic stellate cells during fibrosis (Bachem et al., 1993; de Bleser et al., 1995; Weiner et al., 2000).

Imatinib (STI 571, Gleevec) is employed in the treatment of chronic myelogenous leukemia and gastrointestinal stromal tumors (von Mehren, 2005). It inhibits several tyrosine kinases that are mutated during cancer development. In addition, imatinib is a potent inhibitor of PDGF-B receptor kinase. Consequently, imatinib has been tested for its antifibrotic effect in cultured HSC (Kinnman et al., 2001; Yoshiji et al., 2005) and has recently been evaluated in different animal models of liver fibrosis (Yoshiji et al., 2005; Neef et al., 2006). The fundamental role that PDGF signaling appears to play in liver fibrogenesis has made it an attractive therapeutic target for the treatment of liver fibrosis (Bataller and Brenner, 2005).

In the present study, we have investigated whether the antifibrotic effects of a PDGF tyrosine kinase inhibitor can be enhanced by local delivery to HSC. Drug targeting can improve the effect of a drug by increasing local concentrations at the target site and by providing slow local drug release. In addition, it can prevent side effects in other tissue or organs. PDGF tyrosine kinase activity plays a role in many physiological processes and its

JPET #114496

inhibition by imatinib may lead to side effects like cardiotoxicity, as reported recently (Kerkela et al., 2006).

To effectuate local delivery within HSC in the liver, we have developed a new drug targeting construct, PAP19-M6PHSA, in which a PDGF kinase inhibitor is coupled to the HSC-directed carrier protein mannose-6-phosphate-human serum albumin (M6PHSA). M6PHSA is a well-established carrier that binds to the M6P/IGFII receptor on HSC and accumulates rapidly and extensively in the liver of fibrotic rats (Beljaars et al., 1999). **Figure 1** schematically depicts the structure of the PAP19-M6PHSA conjugate, as well as the structures of imatinib and PAP19, the PDGF kinase inhibitor used in the present study. Zimmermann *et al* have evaluated a series of phenyl-amino-pyrimidine (PAP) derivatives closely related to imatinib (Zimmermann et al., 1997). Among the evaluated derivatives, PAP19 showed an inhibitory profile similar to imatinib with equivalent potency versus PDGF receptor kinase. We now have conjugated PAP19 to M6PHSA employing a novel type of platinum linker chemistry called ULS™ (Universal Linkage System). ULS allows stable coupling of drug molecules to M6PHSA based on the formation of a platinum-ligand coordination bond (Gonzalo et al., 2006). Application of this novel linker technology was essential since it appears to be a straightforward and reliable method for linking PAP19 molecules to the carrier, allowing high synthesis yields in a relative simple approach. Second, the developed PAP19-M6PHSA conjugates display a unique behavior of slow release of drug molecules during a period of days, within the designated target cells.

In the present study, we describe the development of PAP19-M6PHSA and its impact on liver fibrogenesis *in vitro* and *in vivo*. Cultured HSC and fibrotic liver slices were employed as *in vitro* systems to prove the antifibrotic effect of PAP19 and PAP19-M6PHSA. In addition, PAP19-M6PHSA was tested in a rat model of liver fibrosis to study its distribution to the liver and its effects on the development of liver fibrosis.

JPET #114496

Methods

Materials.

The Protein Tyrosine Kinase Inhibitor PAP19 (4-Chloro-N-[4-methyl-3-(4-pyridin-3-yl-pyrimidin-2-ylamino)-phenyl]-benzamide) was kindly provided by György Kéri (Vichem Chemie Research Ltd., Budapest, Hungary). M6PHSA was prepared as described previously (Gonzalo, et al., 2006). Cis-[Pt(ethylenediamine)nitrate-chloride] (ULS) was prepared as previously described (Gonzalo et al., 2006).

Synthesis of PAP19-ULS-M6PHSA.

PAP19-ULS was synthesized and purified by Kreatech Biotechnology (Amsterdam, The Netherlands). In brief, PAP19 (7.2 μ mol, 3 mg; 10 mg/ml in dimethylformamide (DMF)) was mixed with an equimolar amount of ULS (7.2 μ mol, 2.4 mg; 20 mM in DMF). The reaction mixture was heated at 37°C for 24h after which consumption of the starting material was monitored by analytical HPLC. An additional amount of ULS was added (0.5 equivalent, 3.6 μ mol) and the reaction was continued for 48h at 37°C. The crude mixture was concentrated under reduced pressure and dissolved in methanol (600 μ l). The crude product was purified by preparative HPLC and the collected peaks of the main product were taken to dryness under reduced pressure. The resulting white solid was treated with water to remove inorganic salts and dried. Yield: 0.9 mg (20%). Mass spectrometry analysis confirmed the presence of the 1:1 PAP19-ULS species.

^1H NMR of **PAP19** (CD_3OD): δ_{H} 2.33 (s, 3H, CH_3), 7.26 (d, $J = 8.28$ Hz, 1H, CCH_3CH), 7.37 (m, 2H, CHCl), 7.52 (m, 3H, $\text{N}(\text{CH})_2\text{CCCH}$), 7.93 (d, $J = 8.60$ Hz, 2H, CHCHCl), 8.22 (s, 1H, NHCCHC), 8.47 (d, $J = 5.23$ Hz, 1H, CHNCNH), 8.64 (m, 2H, $\text{CH}(\text{CH})_2\text{C}$ and CHCHCNH), 9.29 (s, 1H, NCHC) ppm.

JPET #114496

^1H NMR of **PAP19-ULS** (CD_3OD): δ_{H} 2.27 (m, 3H, CH_3), 2.66 (m, 2H, CH_2), 2.74 (m, 2H, CH_2), 7.15 (m, 3H, CHCCH_3 and CHCl), 7.47 (m, 3H, $\text{N}(\text{CH})_2\text{CCCH}$), 7.84 (d, $J = 5.23$ Hz, 1H, CHCHCNH), 7.89 (m, 2 H, CHCHCl), 8.39 (d, $J = 3.95$ Hz, 1H, CHNCNH) ppm.

Mass spectrometry of PAP19-ULS (ESI+): calculated mass: 705 (m/z); detected masses: 706 $[\text{M}]^+$, 688 $[\text{M}-\text{Cl}^+ + \text{OH}^-]^+$, 670 $[\text{M}-\text{Cl}^- - \text{H}^+]^+$, 669 $[\text{M}-\text{Cl}^- - \text{H}^+]^+$, 651 $[\text{M}-\text{Cl}^- - \text{Cl}^- + \text{OH}^- + \text{H}]^+$.

HPLC analysis: Separations were performed on a Luna2 C18 column. The mobile phase consisted of a binary solvent system of triethylammonium acetate (100 mM pH 5.0):acetonitrile 90:10 (solvent A) and triethylammonium acetate (100 mM pH 5.0):acetonitrile 70:30 (solvent B). The column was eluted at a flow rate of 1.1 mL/min. Compounds were eluted at a stepwise gradient (0 % B from 0-4 min; 0-46 % B from 4-17 min; 46-100 % B from 17-19 min; 100 % B from 19-25 min; 100-0%B from 25-27 min; 0 % B from 27-34 min). PAP19 eluted at 21.2 min (60.8 % B) and PAP19-ULS eluted at 11.5 min (26.5 % B).

PAP19-ULS was conjugated to M6PHSA according to a general protocol that has been described elsewhere for the synthesis of Pentoxifylline-ULS-M6PHSA (Gonzalo et al., 2006). Briefly, PAP19-ULS (143 nmol, 1.6 mg that was dissolved in DMF/ H_2O at 6.7 mg/ml) was added in 10-fold molar excess to M6PHSA (14.3 nmol, 10 mg, dissolved in 1 ml of 20 mM tricine/ NaNO_3 buffer pH 8.3) and reacted overnight at 37°C. The final product was dialyzed against PBS at 4°C, sterilized by filtration via a 0.2 μm filter and stored at -20°C. Protein content was assessed by the BCA assay (Pierce, Rockford, IL, USA). PAP19-M6PHSA and M6PHSA were analyzed by size-exclusion chromatography and anion exchange chromatography as described before (Beljaars et al., 1999) to verify that coupling of PAP19-ULS did not alter the properties of the M6PHSA protein. The amount of PAP19 coupled to M6PHSA was analyzed by isocratic HPLC after competitive displacement of the drug by overnight incubation at 80°C with excess of potassium thiocyanate (KSCN, 0.5M in

JPET #114496

PBS). Elutions were performed on a Waters system (Waters, Milford, MA, USA) equipped with a 5 μm Hypersil BDS C8 column (250x4.6 mm, Thermoquest Runcorn, UK), a thermostated column oven operated at 40°C and an UV detector operated at 269 nm. The mobile phase consisted of acetonitrile/water/trifluoroacetic acid (40/60/0.1, pH 2) at a flow rate of 1.0 ml/min with a sensitivity of 0.01. Retention times: PAP19: 7 min. Chromatograms were also monitored for PAP19-ULS (Retention time: 5 min) to confirm that drug release was complete.

Cells

Hepatic stellate cells were isolated and cultured as described elsewhere (Gonzalo et al., 2006). Cells were split after 3 days and cultured until day 10 to obtain the activated HSC phenotype, and culture activated HSC were used for the experiments described below.

Cell viability studies.

Activated HSC (10,000 cells/well seeded in 96 well-plates, Corning) were washed with serum-free medium and incubated for 24h in medium supplemented with PAP19-M6PHSA (0.1 or 1 mg/ml, corresponding to 10 or 100 μM PAP19 or ULS linker) or with free PAP19, free ULS or unmodified M6PHSA at equimolar concentrations. To evaluate the sensitivity of HSC to platinum toxicity, cells were incubated with cisplatin for 24h. Cell viability was assayed by Alamar blue assay (Serotec, Oxford, UK) according to the supplier's instructions.

Effects on gene expression.

The potential antifibrotic activity of PAP19-M6PHSA and PAP19 was evaluated in cultured HSC and in precision-cut liver slices prepared of fibrotic rat livers (BDL3 rats, i.e. 3 weeks after bile duct ligation). Activated HSC were incubated with indicated compounds for 24h, after which they were processed for RNA analysis as described below. A total of four

JPET #114496

independent experiments were performed in HSC cultures from four different Wistar male rats.

Precision-cut liver slices were prepared as described elsewhere (Olinga et al., 2001; van de Bovenkamp et al., 2005). After 2h of preincubation in William's medium E (Gibco, Life technologies Ltd., Paisley, Scotland, UK) supplemented with D-glucose (25mM) and gentamycin (50 µg/ml) and saturated with 95% O₂, 5% CO₂ at 37°C, slices were transferred into fresh medium and incubated individually in six-well plates with the indicated compounds for 24h, after which they were snap-frozen in liquid nitrogen and stored at -80°C until real-time PCR analysis. Each measurement was performed on three liver slices from the same liver and the experiment was repeated on livers from three different BDL3 rats.

Animal experiments

All animal studies were approved by the local committee for care and use of laboratory animals at Groningen University, and were performed according to strict governmental and international guidelines on animal experimentation. Animals had free access to tap water and standard lab chow and were housed in a 12h/12h light/dark cycle. All the animals included in these studies were monitored by analysis of liver/body weight ratio and biochemical parameters reflecting liver functions like serum bilirubin levels, alanine aminotransferase (ALT) and alkaline phosphatase (AP) levels. These analyses were performed at the University Medical Center Groningen by standard biochemical procedures.

BDL model

Liver fibrosis was induced in male Wistar rats (250 g, Harlan, Zeist, The Netherlands) by bile duct ligation as described previously (Beljaars, et al., 1998). Animals were allowed to recover and carefully observed until final sacrifice at the end of the experiments.

JPET #114496

Experimental protocol

At day 10 after BDL, rats received a single intravenous injection of PAP19-M6PHSA (3.3 mg/kg, corresponding to 150 µg PAP19/kg). Control animals were injected with an equivalent volume of the vehicle (saline, 250 µl). Animals were sacrificed 2h post injection to determine initial accumulation of the conjugate within the liver or were sacrificed 24h or 48h post injection to determine the effects of the conjugate on liver fibrosis. Organs were harvested and processed for drug analysis, RNA isolation and immunohistochemical analysis as described below.

Analysis of PAP19 levels in the liver

Drug levels in the liver were determined according to the HPLC method described above. In brief, approximately 400 µg of liver tissue was accurately weighed and homogenized in 2 ml of PBS using an Ultraturrax. One-fourth of the sample was incubated overnight at 80°C with 500 mM KSCN to release PAP19. The drug was extracted twice with diethyl ether, after which the organic layer was evaporated to dryness and reconstituted in 150 µl of mobile phase. Drug levels were expressed as percentage of the total amount of administered PAP19 that had accumulated in the liver.

RNA isolation and gene expression analysis

Total RNA isolation and synthesis of cDNA was performed according to standard procedures. Quantitative Real-time RT-PCR was performed in duplicate on a ABI 7900HT system (Applied Biosystems, Foster City, CA) using SYBR green primers. For each sample, 1 µl of cDNA was mixed with 0.4 µl of each gene-specific primer (50 µM), 0.8 µl DMSO, 8.4 µl water and 10 µl SYBR Green PCR Master Mix. The housekeeping gene Glyceraldehyde-3-phosphate dehydrogenase (GAPDH) was used as a reference gene and for normalization of the other genes, while ultra pure water was used as a negative control.

Table 1 lists the primers that have been used to investigate antifibrotic responses. PCR

JPET #114496

reactions consisted of 40 cycles (denaturation 15 s 95°C, annealing 15 s 56°C, extension 40 s 72°C). The formation of single products was confirmed by analyzing the dissociation step at the end of each PCR reaction. Data were analyzed with the SDS 2.1 software program (Applied Biosystems). The relative amount of the designated PCR product was calculated by the comparative threshold cycle (CT) method and referred to control treatment.

Immunohistochemical analyses

Cryostat sections (4 μ m) of liver, heart, kidney, lung and spleen were acetone-fixed and stained for the presence of the PAP19-M6PHSA conjugate with an antibody directed against HSA (Cappel ICN Biomedicals, Zoetermeer, The Netherlands) as described elsewhere (Beljaars et al., 1998). Expression of PDGF receptor and its phosphorylation in BDL liver cryosections were investigated by staining with anti-PDGFR- β and anti phospho-PDGFR- β (Santacruz Biotechnology).

The degree of hepatic fibrosis was estimated by staining for collagens using the picro-sirius-red dye (Sigma). Fibrogenic myofibroblasts stained with anti-smooth muscle α actin (α SMA, Sigma, Gillingham, UK). Microphotographs were taken with an optic microscope (Olympus BX40) connected to a high-resolution camera (Olympus Camedia C-5050 zoom) at an original magnification of 4x10. Stainings were quantified by morphometric analysis of the sections using the Image J software package (NIH, Bethesda, ML, USA) and images were captured following automatic white balance and light intensity equilibration with a 40 \times magnification objective and digitized as RGB 24-bit. After shading correction and interactive thresholding, the selected positive pixels were measured. The positive area was the sum of the area of positive pixels per liver biopsy. Results were calculated as the average area of positive pixels per liver biopsy and divided into each group of animal treatment.

JPET #114496

Statistical analysis.

Results are expressed as the mean of at least three independent experiments \pm SD, unless otherwise indicated. Statistical analysis was performed with an unpaired Student's t-test and differences were considered significant at $p < 0.05$.

JPET #114496

Results

Synthesis and characterization of PAP19-M6PHSA conjugate

When observing the structure of imatinib or the related kinase inhibitor PAP19 (**Figure 1**), it is clear that their structures are mainly composed of aromatic rings. Typically, conjugation reactions for the preparation of a drug-linker adduct aim at carboxyl, hydroxyl, thiol or primary amino groups. Since such functional groups are lacking in imatinib or PAP19, one would need to synthesize a derivatized molecule, which potentially may alter or destroy the pharmacological activity of the inhibitor. We therefore pursued a different strategy in which a novel linker was applied that binds the drug via a coordinative linkage at the pyridyl nitrogen of PAP19. HPLC analysis and mass spectrometry indicated complete derivatization of the drug into the drug-ULS 1:1 product. The PAP19-ULS adduct was subsequently conjugated to M6PHSA and the final high-molecular weight product was extensively purified by dialysis, which also removed free PAP19-ULS molecules not linked to the carrier (HPLC analysis, data not shown). An average of eight PAP19-ULS molecules was coupled per M6PHSA, as assessed by HPLC after release of the drug from the carrier. The overall yield of the final reaction step was 84%. Conjugation of PAP19 to M6PHSA did not change the charge or size features of M6PHSA, as determined by anion-exchange chromatography and size exclusion chromatography, respectively (**Figure 2**).

Effects in cultured hepatic stellate cells and fibrotic liver slices

The use of a platinum(II) compound as a linker may introduce platinum-associated effects in the drug targeting preparation. We therefore evaluated HSC viability in the presence of PAP19-M6PHSA conjugate or its respective components PAP19, ULS linker or M6PHSA carrier. At high concentrations (100 μ M), both free cisplatin and ULS linker displayed toxic effects. PAP19-M6PHSA at equivalent platinum concentrations did not affect HSC viability

JPET #114496

(Figure 3). Neither free drug nor unmodified M6PHSA reduced HSC viability, although PAP19 at the highest concentration even increased the number of HSC.

To examine the potential antifibrotic effects of PAP19-M6PHSA conjugate and non-conjugated PAP19, we investigated their effects on the expression of fibrosis related genes in cultured HSC and fibrotic liver slices. Both PAP19-M6PHSA and free PAP19 downregulated the expression of α SMA and collagen 1a1 in cultured HSC (**Figure 4A**). In contrast, M6PHSA did not affect the expression of these genes in HSC. The other genes that were examined, PDGF receptor- β and TIMP-1, were not significantly reduced by either treatment.

Precision cut liver slices were prepared from rats that had undergone bile duct ligation three weeks before, and thus encompassed all liver cell types in the context of a fibrotic extracellular matrix. In agreement with the results in cultured HSC, PAP19-M6PHSA and PAP19 showed pronounced reductions in the expression of α SMA and collagen 1a1 (**Figure 4B**). In addition, PDGFR- β (PAP19-M6PHSA and PAP19) and TIMP-1 (PAP19) gene levels were inhibited significantly in slices, while those genes were not affected in cultured HSC. Furthermore, M6PHSA carrier showed inhibitory effects on some of the investigated genes, although TIMP-1 expression was enhanced by M6PHSA. Differences between PAP19-M6PHSA were significant for α SMA and collagen 1a1. These results encouraged us to evaluate PAP19-M6PHSA in an animal model of liver fibrosis.

Animal studies.

To demonstrate that PAP19-M6PHSA was capable of homing to the fibrotic liver and that the compound is capable of inhibiting early stages of fibrogenesis, BDL rats at day 10 after ligation of the bile were treated with a single dose of the product. In the rat BDL model, HSC activation associated with PDGF receptor expression and downstream signalling is

JPET #114496

prominent at this day (Neef et al., 2006). In addition, the expression of the M6P/IGF-II receptor which recognizing M6P-HSA is also increased at day 10 after BDL (Greupink et al., 2006a).

Table 2 shows the characteristics of the BDL rats included in the studies. The animals were treated with a relatively low dose of PAP19-M6PHSA (1 mg of conjugate/animal), which corresponds to 150 µg/kg of the conjugated drug. Administration of PAP19-M6PHSA did not affect the body weight of the rats, nor did it change the biochemical parameters that were analyzed.

Distribution of PAP19-M6PHSA in fibrotic rats.

Previous studies in our laboratory have demonstrated that M6PHSA extensively binds to activated HSC in the fibrotic liver (Beljaars et al., 1999). Typically, about 60% of the injected carrier accumulated in the fibrotic liver already within 10 min after administration (see for instance (Gonzalo et al., 2006)). In the present study, PAP19-M6PHSA organ distribution was investigated at a later time point, 2h after administration of the product, to allow for a more complete distribution of the conjugate (**Figure 5**). PAP19-M6PHSA was detectable in the liver in a non-parenchymal staining pattern. Although double immunostaining to detect colocalization with HSC failed due to the faint staining (data not shown), these results suggest that PAP19-M6PHSA homed to the liver in a similar manner as other HSC-selective conjugates. PAP19-M6PHSA was undetectable in other organs like heart, kidney, lung and spleen. (**Fig. 5C-F**).

We furthermore quantified the accumulation of PAP19-M6PHSA in the liver by assaying PAP19 levels by HPLC. As can be observed in **Figure 6**, 30% of the injected dose had been accumulated in the liver after 2h, and these drug levels persisted up to the last time point at 48h.

JPET #114496

Effects of PAP19-M6PHSA in fibrotic rats.

Antifibrotic effects of PAP19-M6PHSA were studied at the latter two time points of the study, 24h and 48h after administration of the conjugate, respectively. First, we investigated whether PAP19-M6PHSA affected fibrotic gene expression in a similar approach as described above for cultured HSC and precision-cut slices. We did not observe changes in the expression of fibrosis reporter genes (data not shown). Immunohistochemical staining of fibrotic markers, however, clearly indicated the establishment of fibrosis and the pharmacological activity of PAP19-M6PHSA. Sirius Red staining for collagen showed a continuous increment in deposited extracellular matrix components from day 10 to 12 after bile duct ligation (**Figure 7A**). Treatment with a single dose of PAP19-M6PHSA significantly attenuated collagen deposition at both 24h and 48h after administration. Apart from reduced staining intensity, the antifibrotic effect of PAP19-M6PHSA was illustrated by a reduced portal-portal bridging in fibrotic areas (**Figure 7B**). Similarly, treatment with PAP19-M6PHSA significantly attenuated the α SMA stained area in the liver at both 24h and 48h after single dose treatment (**Figure 8**).

JPET #114496

Discussion

Liver fibrosis is in principle a reversible process in which the stellate cells have been identified as the key fibrogenic cells (Friedman, 2003). PDGF is the most potent mitogen for HSC *in vitro*, and it plays an important role in the transformation of HSC into myofibroblast-like cells *in vivo* (Pinzani et al., 1994). Targeting the PDGF signaling cascade therefore represents a promising antifibrotic approach. Several recent studies have described the antifibrogenic properties of the kinase inhibitor imatinib in different models of fibrotic disease (Lassila et al., 2005; Wang et al., 2005; Yoshiji et al., 2005). On the other hand, concerns have been raised in relation to the effectiveness of imatinib as an antifibrogenic drug (Neef et al., 2006; Vittal et al., 2007), especially in later stages of liver fibrosis. In the present study, the new product PAP19-M6PHSA was designed to effectively and specifically deliver a imatinib-related kinase inhibitor to HSC, in order to improve its antifibrotic properties. We demonstrate the antifibrogenic effects of PAP19-M6PHSA in two different validated *in vitro* systems and furthermore show the sustained delivery of the drug within the liver, as well as its potential activity in rats with liver fibrosis.

PAP19 is a potent inhibitor of PDGR-kinase with an IC₅₀ of 10 nM (Zimmermann et al., 1997). We confirmed the antifibrotic potential of PAP19 by incubating culture-activated HSC and BDL liver slices with the drug. Our results with PAP19 are in good agreement with prior studies in which imatinib was tested for its activity in HSC (Yoshiji et al., 2005) or liver slices (van de Bovenkamp et al., 2006). Imatinib dose-dependently inhibited fibrotic gene expression in slices, reaching 70-80% inhibition of collagen1a1 and α SMA at 10 μ M (van de Bovenkamp et al., 2006). No toxicity of imatinib was observed in fibrotic slices. In PDGF-stimulated HSC, 10 μ M of imatinib blunted the expression of α SMA, α 2-(I)-procollagen, in addition to an almost complete inhibition of PDGF-induced proliferation and migration (Yoshiji et al., 2005). We did not add external PDGF to our experiments, but it

JPET #114496

has been reported that the growth factor is synthesized *in situ* by activated HSC in culture or in slices (Pinzani, 2002). We also found that PAP19 reduced PDGFR- β and TIMP-1 expression in BDL slices. TIMP-1 expression is increased during liver fibrosis and plays an important role in liver fibrogenesis by modulating extracellular matrix remodeling (Iredale et al., 1998). Taken together, these data support our hypothesis that PAP19 is a proper candidate for HSC directed drug delivery.

PAP19-M6PHSA potently inhibited fibrotic gene expression in both HSC and fibrotic liver slices. These results are remarkable taking into account that carrier-bound drug most likely should be released from the carrier to become active. First, the attachment of PAP19 to ULS and subsequently to the carrier will prevent the pharmacological activity of PAP19 since the active site of the drug is blocked by the linker. Intracellular release of the compound will revert PAP19-M6PHSA to the active kinase inhibitor. Second, drug-M6PHSA conjugates can not diffuse across cell membranes but will enter cells by receptor mediated endocytosis, followed by lysosomal routing (Beljaars et al., 2001). On the other hand, the kinase domain of the PDGF receptor is located in the cytosol. Thus, the conjugate will not end up in the same intracellular compartment as the pharmacological target of PAP19. We postulate that the conjugate is degraded efficiently in the lysosomes of HSC and during this process drug will be released from the carrier. A possible mechanism by which drug release can take place is competitive displacement by glutathione or other endogenous compounds that can coordinate to platinum (Gonzalo et al., 2006; Prakash et al., 2006; Temming et al., 2006a; Temming et al., 2006b).

Rapid degradation of the conjugate within the lysosomal compartment of target cells also explains the faint staining of PAP19-M6PHSA in the liver after its administration to BDL rats. To allow for a more complete accumulation of the conjugate within the liver, we had sacrificed the animals at a rather late time point (2h) as compared to other studies from our

JPET #114496

group in which staining was performed 10-20 min after administration (Gonzalo et al., 2006; Greupink et al., 2006b; Hagens et al., 2007). Most likely, this prolonged period allowed for the uptake and degradation of the carrier by target cells, while the majority of the compound will be bound extracellularly or in the endosomes at the 10-20 min time point. As a consequence, anti-HSA staining resulted in poor immunodetection of the PAP19-M6PHSA conjugate. However, the analysis of the coupled drug by HPLC clearly showed the efficient accumulation of PAP19-M6PHSA in the liver. Furthermore, the persistence of high drug levels even at 2 days after its administration denotes that PAP19 is retained within the fibrotic liver. This result is in good agreement with the results of another drug-ULS construct aimed at the kidney, which could be detected up to 3 days after single dosing (Prakash et al., 2006). Whether the released PAP19 molecules will be retained within HSC or redistribute to other cell types within the liver is presently unknown. Although one may argue that redistribution of the delivered drug is unfavorable, it may also help in reaching pro-fibrogenic liver cell types such as peribiliary fibroblasts. Highest drug levels can be expected however in target cells that have accumulated and internalized the conjugate. Of note, the drug delivery strategy greatly lowered the systemic distribution of imatinib, since a much lower dose was administered than commonly applied for liver fibrosis treatment, 150 $\mu\text{g}/\text{kg}$ as a single dose versus 5-20 mg/kg daily, respectively. This lower dose was furthermore accumulated preferentially within the fibrotic liver. As a consequence, potential side-effects of imatinib in non-fibrotic tissues will be avoided, which seems relevant in view of the reported cardiotoxicity of imatinib (Kerkela et al., 2006).

Eventually, released PAP19 should effectuate a sustained blockade of PDGF kinase activity within the fibrotic liver. Staining for phosphorylated PDGF receptor in untreated BDL rats at day 10 after ligation was however scattered and did not match the pattern of total PDGF receptor (unpublished results). This may relate to a technical problem as the commercially

JPET #114496

available antibodies were not reported for immunostaining of fibrotic tissues. Yoshiji *et al* have reported on the capability of imatinib to inhibit PDGF receptor phosphorylation in HSC (Yoshiji *et al.*, 2005), and the anti-PDGF kinase activity of PAP19 has been well documented (Zimmermann *et al.*, 1997). Since pharmacological activity of PAP19-M6PHSA is observed in HSC and fibrotic slices, it is feasible that kinase inhibition has occurred in the cells that have accumulated PAP19-M6PHSA. Although this could not be directly demonstrated, the pharmacological effects of the construct found *in vivo* are in accordance with this.

After single administration, PAP19-M6PHSA markedly reduced collagen deposition together with a suppression of α SMA-positive cells which reflects a reduction in the number of activated HSC (Olaso and Friedman, 1998). In contrast to the effects on protein expression of fibrotic markers, PAP19-M6PHSA administration did not affect the gene expression of such markers in BDL rats. This discrepancy either reflects different sensitivity of the assays, or corresponds to a greater reduction of collagen and α SMA at the protein level than at gene expression level. This divergence has previously been described in experiments investigating the inhibition of hepatic fibrosis (Yata *et al.*, 2002), and might be due to post-transcriptional regulation of collagen expression in cultured HSC (Stefanovic *et al.*, 1997).

Several other approaches for blockade of the PDGF signalling cascade have been investigated as a strategy to block liver fibrosis. Some papers showed that monoclonal antibodies directed against the extracellular domain of the PDGF receptor can prevent binding of the PDGF ligand, thereby inhibiting mitogenic signalling (Heldin, 1997; Shulman *et al.*, 1997). In a different strategy, Borkham-Kamphorst and colleagues produced a soluble PDGF receptor which was capable of reducing ECM deposition in the BDL model after daily administration for fourteen days (Borkham-Kamphorst *et al.*, 2004). Consistent with

JPET #114496

this, short-term treatment with imatinib in the BDL model caused a marked reduction in HSC proliferation (Kinnman et al., 2001). According to Neef and colleagues, the effect of imatinib is limited to the early phase of fibrogenesis, due to the lack of efficiency in advanced liver injury, i.e., 3 to 4 weeks after BDL (Neef et al., 2006). In contrast to this latter observation, another study reported a pronounced inhibition of SMA-positive fibroblast and expression of fibrosis markers after 8 weeks of imatinib administration to fibrotic rats (Yoshiji et al., 2005). These authors studied the effect of imatinib in the pig-serum induced model of liver fibrosis, which is characterized by a slow progression of fibrogenesis, resembling the human situation. Thus, it might be a relevant therapy in patients with early stages of liver fibrosis.

In conclusion, we have evaluated a new strategy for local delivery of a PDGF kinase inhibitor to the fibrotic liver. Our strategy differs completely from the above listed studies in which the free drug imatinib is used. We employed a carrier molecule that is internalized by target HSC, after which the kinase inhibitor is released inside the cells. The delivered kinase inhibitor produced a significant effect on the fibrotic process 24 to 48 hours after its administration to BDL rats. These results illustrate the potential of employing PAP19-M6PHSA as a cell-specific drug that may effectively lead to reduced activation of HSC and consequently may reduce liver fibrosis.

JPET #114496

Acknowledgements

Jan Visser and Jai Prakash (University of Groningen, The Netherlands) are kindly acknowledged for assistance in HPLC analysis and colleagues at Kreatech for critical reading of the manuscript.

JPET #114496

References

Bachem MG, Meyer D, Schafer W, Riess U, Melchior R, Sell KM and Gressner AM (1993)

The response of rat liver perisinusoidal lipocytes to polypeptide growth regulator changes with their transdifferentiation into myofibroblast-like cells in culture. *J Hepatol* **18**:40-52.

Bataller R and Brenner DA (2005) Liver fibrosis. *J Clin Invest* **115**:209-218.

Beljaars L, Poelstra K, Molema G and Meijer DK (1998) Targeting of sugar- and charge-modified albumins to fibrotic rat livers: the accessibility of hepatic cells after chronic bile duct ligation. *J Hepatol* **29**:579-588.

Beljaars L, Molema G, Weert B, Bonnema H, Olinga P, Groothuis GM, Meijer DK and Poelstra K (1999) Albumin modified with mannose 6-phosphate: A potential carrier for selective delivery of antifibrotic drugs to rat and human hepatic stellate cells. *Hepatology* **29**:1486-1493.

Beljaars L, Olinga P, Molema G, de Bleser P, Geerts A, Groothuis GM, Meijer DK and Poelstra K (2001) Characteristics of the hepatic stellate cell-selective carrier mannose 6-phosphate modified albumin (M6P(28)-HSA). *Liver* **21**:320-328.

Borkham-Kamphorst E, Herrmann J, Stoll D, Treptau J, Gressner AM and Weiskirchen R (2004) Dominant-negative soluble PDGF-beta receptor inhibits hepatic stellate cell activation and attenuates liver fibrosis. *Lab Invest* **84**:766-777.

JPET #114496

de Bleser PJ, Jannes P, van Buul-Offers SC, Hoogerbrugge CM, van Schravendijk CF, Niki T, Rogiers V, van den Brande JL, Wisse E and Geerts A (1995) Insulinlike growth factor-II/mannose 6-phosphate receptor is expressed on CCl4-exposed rat fat-storing cells and facilitates activation of latent transforming growth factor-beta in cocultures with sinusoidal endothelial cells. *Hepatology* **21**:1429-1437.

Friedman SL (1999) The virtuosity of hepatic stellate cells. *Gastroenterology* **117**:1244-1246.

Friedman SL (2003) Liver fibrosis -- from bench to bedside. *J Hepatol* **38 Suppl 1**:S38-53.

Gonzalo T, Talman EG, van de Ven A, Temming K, Greupink R, Beljaars L, Reker-Smit C, Meijer DK, Molema G, Poelstra K and Kok RJ (2006) Selective targeting of pentoxifylline to hepatic stellate cells using a novel platinum-based linker technology. *J Control Release* **111**:193-203.

Greupink R, Bakker HI, van Goor H, de Borst MH, Beljaars L and Poelstra K (2006a) Mannose-6-phosphate/insulin-Like growth factor-II receptors may represent a target for the selective delivery of mycophenolic acid to fibrogenic cells. *Pharm Res* **23**:1827-1834.

Greupink R, Reker-Smit C, Proost JH, Weemaes AM, de Hooge M, Poelstra K and Beljaars L (2006b) Pharmacokinetics of a hepatic stellate cell-targeted doxorubicin construct in bile duct-ligated rats. *Biochem Pharmacol* in press.

JPET #114496

Hagens WI, Mattos A, Greupink R, de Jager-Krikken A, Reker-Smit C, van Loenen-Weemaes A, Gouw AS, Poelstra K and Beljaars L (2007) Targeting 15d-Prostaglandin J(2) to Hepatic Stellate Cells: Two Options Evaluated. *Pharm Res* in press.

Heldin CH (1997) Simultaneous induction of stimulatory and inhibitory signals by PDGF. *FEBS Lett* **410**:17-21.

Iredale JP, Benyon RC, Pickering J, McCullen M, Northrop M, Pawley S, Hovell C and Arthur MJ (1998) Mechanisms of spontaneous resolution of rat liver fibrosis. Hepatic stellate cell apoptosis and reduced hepatic expression of metalloproteinase inhibitors. *J Clin Invest* **102**:538-549.

Kerkela R, Grazette L, Yacobi R, Iliescu C, Patten R, Beahm C, Walters B, Shevtsov S, Pesant S, Clubb FJ, Rosenzweig A, Salomon RN, Van Etten RA, Alroy J, Durand JB and Force T (2006) Cardiotoxicity of the cancer therapeutic agent imatinib mesylate. *Nat Med* **12**:908-916.

Kinnman N, Gorla O, Wendum D, Gendron MC, Rey C, Poupon R and Housset C (2001) Hepatic stellate cell proliferation is an early platelet-derived growth factor-mediated cellular event in rat cholestatic liver injury. *Lab Invest* **81**:1709-1716.

Lassila M, Jandeleit-Dahm K, Seah KK, Smith CM, Calkin AC, Allen TJ and Cooper ME (2005) Imatinib attenuates diabetic nephropathy in apolipoprotein E-knockout mice. *J Am Soc Nephrol* **16**:363-373.

JPET #114496

Neef M, Ledermann M, Saegesser H, Schneider V, Widmer N, Decosterd LA, Rochat B and Reichen J (2006) Oral imatinib treatment reduces early fibrogenesis but does not prevent progression in the long term. *J Hepatol* **44**:167-175.

Olaso E and Friedman SL (1998) Molecular regulation of hepatic fibrogenesis. *J Hepatol* **29**:836-847.

Olinga P, Merema MT, de Jager MH, Derks F, Melgert BN, Moshage H, Slooff MJ, Meijer DK, Poelstra K and Groothuis GM (2001) Rat liver slices as a tool to study LPS-induced inflammatory response in the liver. *J Hepatol* **35**:187-194.

Pinzani M (2002) PDGF and signal transduction in hepatic stellate cells. *Front Biosci* **7**:d1720-1726.

Pinzani M, Milani S, Grappone C, Weber FL, Jr., Gentilini P and Abboud HE (1994) Expression of platelet-derived growth factor in a model of acute liver injury. *Hepatology* **19**:701-707.

Prakash J, Sandovici M, Saluja V, Lacombe M, Schaapveld RQ, de Borst M, van Goor H, Henning RH, Proost JH, Moolenaar F, Keri G, Meijer DK, Poelstra K and Kok RJ (2006) Intracellular Delivery of the P38 MAPK Inhibitor SB202190 in Renal Tubular Cells: a Novel Strategy to Treat Renal Fibrosis. *J Pharmacol Exp Ther* **319**:8-19.

Shulman T, Sauer FG, Jackman RM, Chang CN and Landolfi NF (1997) An antibody reactive with domain 4 of the platelet-derived growth factor beta receptor allows BB binding

JPET #114496

while inhibiting proliferation by impairing receptor dimerization. *J Biol Chem* **272**:17400-17404.

Stefanovic B, Hellerbrand C, Holcik M, Briendl M, Aliebbhaber S and Brenner DA (1997) Posttranscriptional regulation of collagen alpha1(I) mRNA in hepatic stellate cells. *Mol Cell Biol* **17**:5201-5209.

Temming K, Lacombe M, Schaapveld RQ, Orfi L, Keri G, Poelstra K, Molema G and Kok RJ (2006a) Rational design of RGD-albumin conjugates for targeted delivery of the VEGF-R kinase inhibitor PTK787 to angiogenic endothelium. *ChemMedChem* **1**:1200-1203.

Temming K, Lacombe M, van der Hoeven P, Prakash J, Gonzalo T, Dijkers EC, Orfi L, Keri G, Poelstra K, Molema G and Kok RJ (2006b) Delivery of the p38 MAPkinase Inhibitor SB202190 to Angiogenic Endothelial Cells: Development of Novel RGD-Equipped and PEGylated Drug-Albumin Conjugates Using Platinum(II)-Based Drug Linker Technology. *Bioconjug Chem* **17**:1246-1255.

Tsukada S, Parsons CJ and Rippe RA (2006) Mechanisms of liver fibrosis. *Clin Chim Acta* **364**:33-60.

van de Bovenkamp M, Groothuis GM, Draaisma AL, Merema MT, Bezuijen JI, van Gils MJ, Meijer DK, Friedman SL and Olinga P (2005) Precision-cut liver slices as a new model to study toxicity-induced hepatic stellate cell activation in a physiologic milieu. *Toxicol Sci* **85**:632-638.

JPET #114496

van de Bovenkamp M, Groothuis GM, Meijer DK and Olinga P (2006) Precision-cut fibrotic rat liver slices as a new model to test the effects of anti-fibrotic drugs in vitro. *J Hepatol* **45**:696-703.

Vittal R, Zhang H, Han MK, Moore BB, Horowitz JC and Thannickal VJ (2007) Effects of the Protein Kinase Inhibitor, Imatinib Mesylate, on Epithelial/Mesenchymal Phenotypes: Implications for Treatment of Fibrotic Diseases. *J Pharmacol Exp Ther* in press.

von Mehren M (2005) Targeted therapy with imatinib: hits and misses? *J Clin Oncol* **23**:8-10.

Wang S, Wilkes MC, Leof EB and Hirschberg R (2005) Imatinib mesylate blocks a non-Smad TGF-beta pathway and reduces renal fibrogenesis in vivo. *Faseb J* **19**:1-11.

Weiner JA, Chen A and Davis BH (2000) Platelet-derived growth factor is a principal inductive factormodulating mannose 6-phosphate/insulin-like growth factor-II receptorgene expression via a distal E-box in activated hepatic stellate cells. *Biochem J* **345 Pt 2**:225-231.

Wong L, Yamasaki G, Johnson RJ and Friedman SL (1994) Induction of beta-platelet-derived growth factor receptor in rat hepatic lipocytes during cellular activation in vivo and in culture. *J Clin Invest* **94**:1563-1569.

Yata Y, Gotwals P, Koteliansky V and Rockey DC (2002) Dose-dependent inhibition of hepatic fibrosis in mice by a TGF-beta soluble receptor: implications for antifibrotic therapy. *Hepatology* **35**:1022-1030.

JPET #114496

Yoshiji H, Noguchi R, Kuriyama S, Ikenaka Y, Yoshii J, Yanase K, Namisaki T, Kitade M, Masaki T and Fukui H (2005) Imatinib mesylate (STI-571) attenuates liver fibrosis development in rats. *Am J Physiol Gastrointest Liver Physiol* **288**:G907-913.

Zimmermann J, Buchdunger E, Mett H, Meyer T and Lydon NB (1997) Potent and selective inhibitors of the Abl-kinase: Phenylamino-pyrimidine (PAP) derivatives. *Bioorganic & Medicinal Chemistry Letters* **7**:187-192.

JPET #114496

Footnotes

a)

This study was supported by grants from SenterNovem (TSGE1083), NWO Science Netherlands (R 02-1719, 98-162).

b)

Address correspondence to:

Robbert J. Kok, PhD

Department of Pharmaceutics, Utrecht Institute for Pharmaceutical Sciences (UIPS),

Sorbonnelaan 16, 3584 CA Utrecht, The Netherlands

Phone: +31-30-253 4724

Fax: +31-30-251-7839

Email: r.j.kok@pharm.uu.nl

c)

¹ Present affiliation for Dr Gonzalo: Department of Pharmaceutics and Pharmaceutical Technology, Faculty of Pharmacy, University of Santiago de Compostela, Spain.

gonzaloteresa@yahoo.es

JPET #114496

Legends for Figures

Figure 1. Structures of the kinase inhibitors imatinib and PAP19 (phenylamino pyrimidine derivative 19) and of the drug targeting conjugate PAP19-M6PHSA. PAP19-ULS-M6PHSA was synthesized by reacting PAP19 via its pyridyl aromatic nitrogen to the linker ULS, which was subsequently linked to mannose-6-phosphate modified human serum albumin (M6PHSA). Typically, each PAP19-M6PHSA conjugate contained 8 drug molecules and approximately 30 mannose-6-phosphate groups, which facilitate binding to activated hepatic stellate cells.

Figure 2. Characteristics of PAP19-M6PHSA drug targeting conjugate.

A. MonoQ anion exchange chromatography confirmed that the charge of the protein was not affected after coupling of PAP19-ULS to the carrier. Both M6PHSA and PAP19-M6PHSA eluted at a later retention time than unmodified HSA due to the negatively charged mannose-6-phosphate groups.

B. Size exclusion chromatography showed the monomeric composition of PAP19-M6PHSA. Notice the similar elution profiles of M6PHSA and PAP19-M6PHSA.

Figure 3. Activated HSC incubated with PAP19-M6PHSA.

Effect of PAP19-M6PHSA and drug, linker and carrier on HSC cell viability, as determined by Alamar Blue assay. Cultured HSC were incubated for 24h with the compounds. Indicated concentrations reflect the platinum content of the tested compounds or equivalent amounts of PAP19 or M6PHSA (*P<0.05).

Figure 4. Effects of PAP19 and PAP19-M6PHSA on the expression of fibrotic genes.

Activated HSC (**A**) and precision-cut slices (**B**) from BDL rats were incubated for 24h with

JPET #114496

PAP19 or PAP19-M6PHSA (both at 10 μ M of drug). M6PHSA was tested in an equivalent concentration of carrier (0.1mg/ml). Gene expressions levels were normalized to the expression levels in control HSC or slices (* P<0.05).

Figure 5. Organ distribution of PAP19-M6PHSA in BDL rats. Immunostaining with anti-HSA was performed on tissue sections from saline treated BDL rats (A) or rats treated with PAP19-M6PHSA that had been sacrificed 2h after single dose administration. **A)** liver of saline treated BDL rat; **B)** liver of PAP19-M6PHSA treated BDL rat, **C-F)** heart, kidney, lung and spleen of PAP19-M6PHSA treated BDL rat. Magnification 20x.

Figure 6. Liver drug levels after single dose treatment with PAP19-M6PHSA. Liver homogenate was treated as described in material and methods to liberate conjugated PAP19 from the linker, followed by HPLC analysis of the parent drug. Drug levels were expressed as percentage of the injected dose by correcting for liver weights and administered dose.

Figure 7. Effect of single dose administration of PAP19-M6PHSA on the deposition of collagen in the liver of BDL rats.

A. Quantification of the area with Sirius Red staining in rat liver specimens (n = 25, mean \pm SD. *P<0.05 versus saline treated group at same day). Day 10, 11, 12 correspond to 2h, 24h and 48h after administration of compounds, respectively. **B.** Representative liver sections processed for sirius-red collagen staining. Rats receiving saline (left panels) showed a marked deposition of collagen, as assessed with Sirius Red, which co-localized with areas with active fibrogenesis. Rats treated with PAP19-M6PHSA (right panels) showed attenuated liver fibrosis development. Magnification 40x.

JPET #114496

Figure 8. Effect of single dose administration of PAP19-M6PHSA on the accumulation of myofibroblasts and activated HSC in BDL rat livers, as assessed by α SMA expression.

A. Quantification of the area with α SMA staining in rat liver specimens (n = 25, mean \pm SD; *P<0.05 vs. saline treated BDL group at same day). Day 10, 11, 12 correspond to 2h, 24h and 48h after administration of compounds, respectively.

B. Representative liver sections processed for α SMA immunohistochemistry. Rats receiving saline (left panels) showed a marked accumulation of α SMA-positive cells, which co-localized with areas with active fibrogenesis. Rats treated with PAP19-M6PHSA (right panels) showed less α SMA-positive cells. Magnification 40x.

Tables

Table 1. Primers used to study fibrotic gene expression.

gene	forward primer	reverse primer	product size
rat smooth muscle α actin	5'-GACACCAGGGAGTGATGGTT -3'	5'-GTTAGCAAGGTCGGATGCTC-3'	202 bp
rat collagen type 1 a1	5'-AGCCTGAGCCAGCAGATTGA-3'	5'-CCAGGTTGCAGCCTTGGTTA-3'	145 bp
rat PDGFR- β	5'-TGTTTCGTGCTATTGCTCCTG -3'	5'-TCAGCACACTGGAGAAGGTG -3'	201 bp
rat timp-1	5'-GAGAGCCTCTGTGGATATGT -3'	5'-CAGCCAGCACTATAGGTCTT -3'	334 bp
rat GAPDH	5'-CGCTGGTGCTGAGTATGTCG-3'	5'-CTGTG GTCATGAGCCCTTCC-3'	179 bp

bp: base pairs

Table 2. Dose regimens, animal data and biochemical parameters from PAP19-M6PHSA single injection study.

	BDL day 10 + saline	BDL day 11 + saline	BDL day 12 + saline	BDL day 10 +PAP19- M6PHSA	BDL day 11 +PAP19- M6PHSA	BDL day 12 +PAP19- M6PHSA
Number of rats	4	4	4	2	4	4
Body weight (g)	250.2 ± 46.7	311.2 ± 14.7	273.4 ± 16.4	280.7 ± 10.1	301.4 ± 14.1	306.4 ± 13.5
Liver/body weight ratio (g/g)	0.055 ± 0.009	0.062 ± 0.007	0.065 ± 0.004	0.061 ± 0.002	0.060 ± 0.006	0.065 ± 0.009
Dose	saline	saline	saline	3.3mg/kg	3.3mg/kg	3.3mg/kg
Bilirubin (µmol/l)	183.7 ± 35.8	178.0 ± 48.2	228.5 ± 18.7	252.3 ± 55.9	136.0 ± 10.0	183.5 ± 27.9
ALT (U/l)	86.3 ± 30.9	79.8 ± 46.1	79.3 ± 11.2	96.5 ± 4.9	72.7 ± 10.6	81.0 ± 17.0
AP (U/l)	391.2 ± 46.4	476.0 ± 162.6	358.3 ± 234.1	458.0 ± 11.2	426.0 ± 101.3	511.3 ± 121.4

Data are shown as mean ± SD. ALT, alanine aminotransferase; AP: alkaline phosphatase.

Figure 1

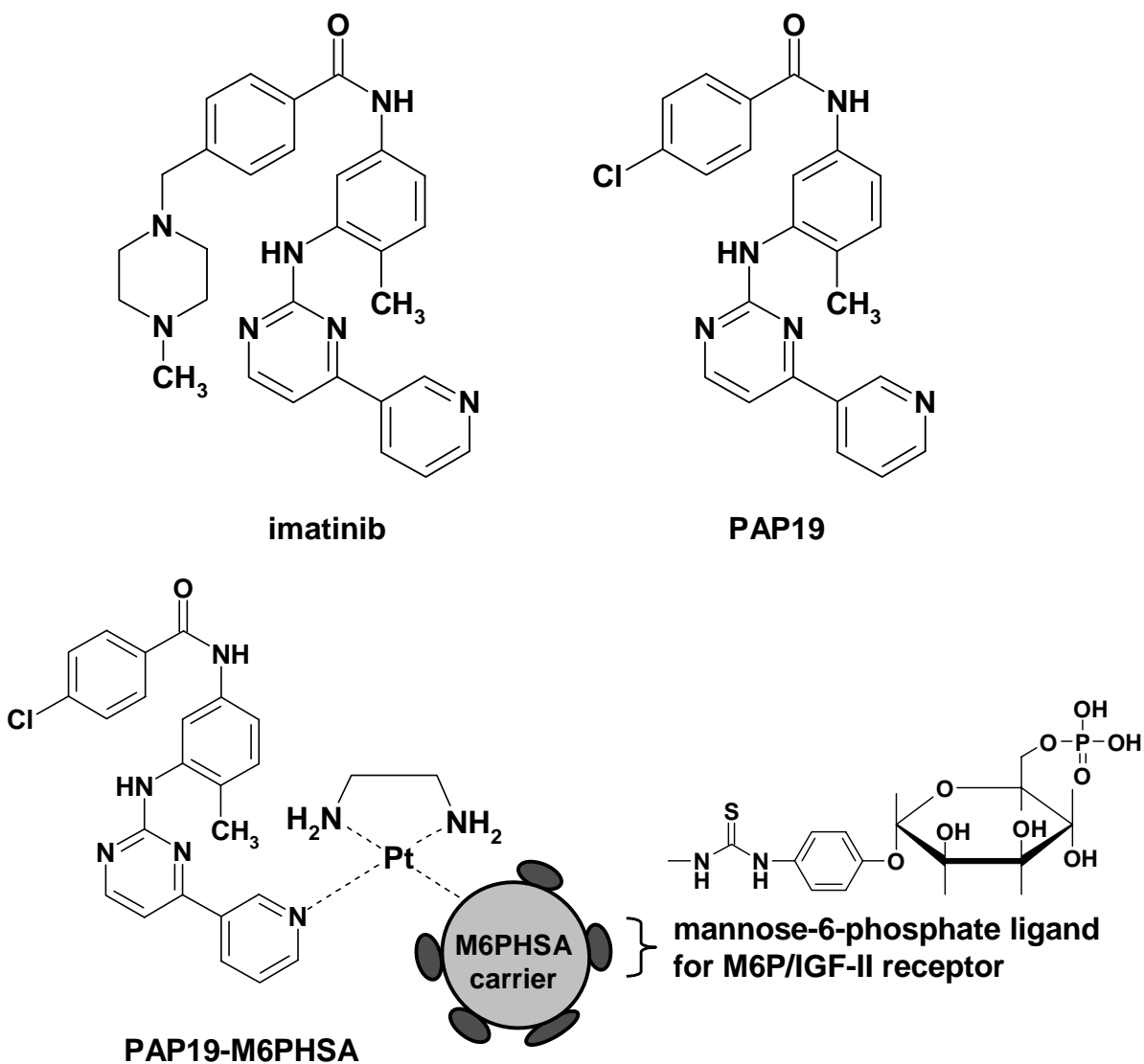
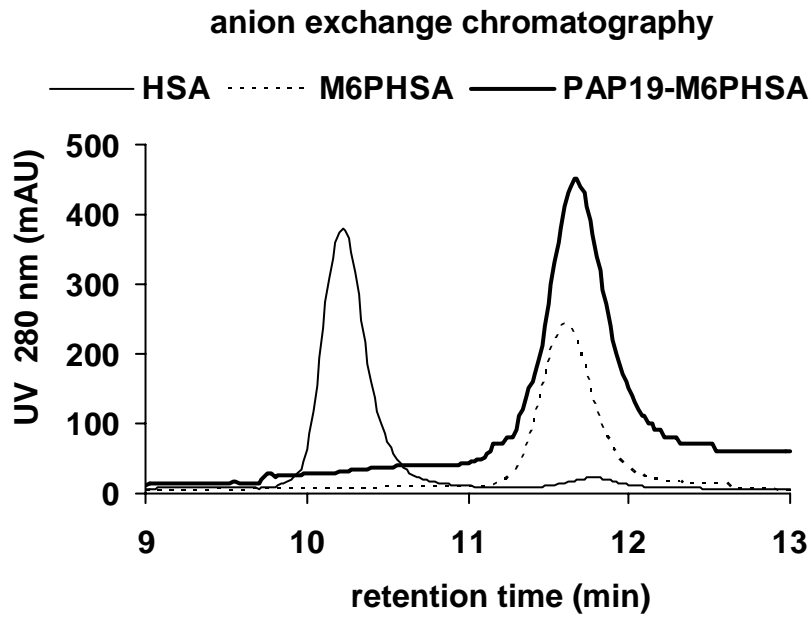


Figure 2

A



B

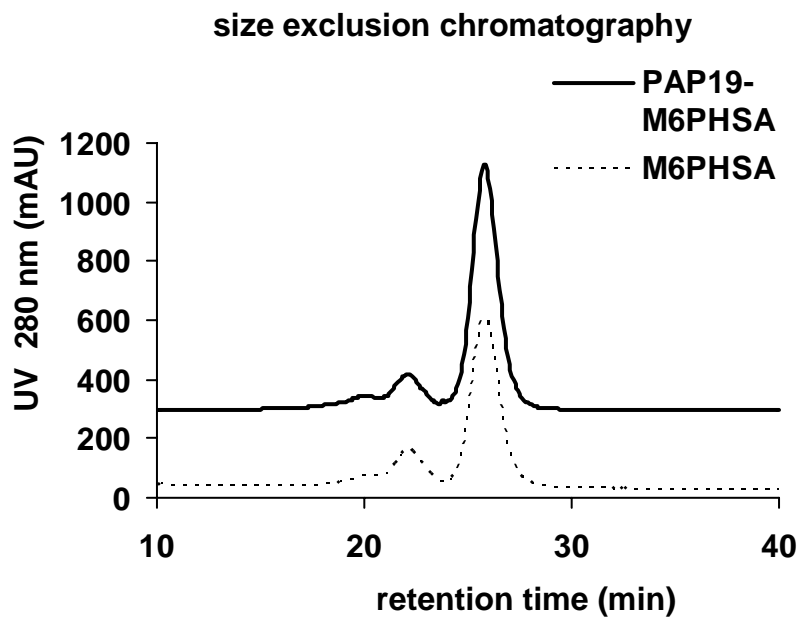


Figure 3

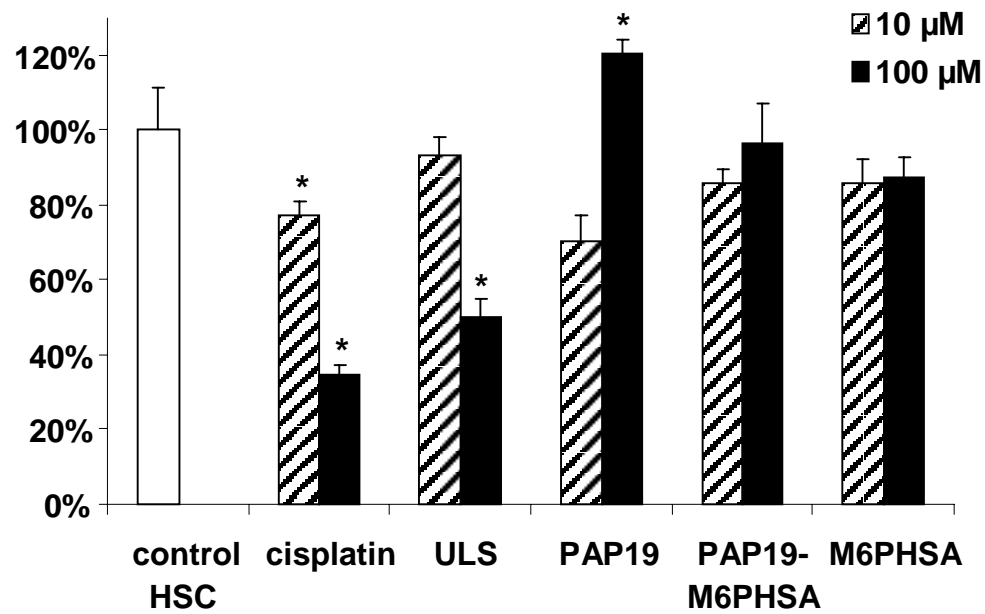


Figure 4

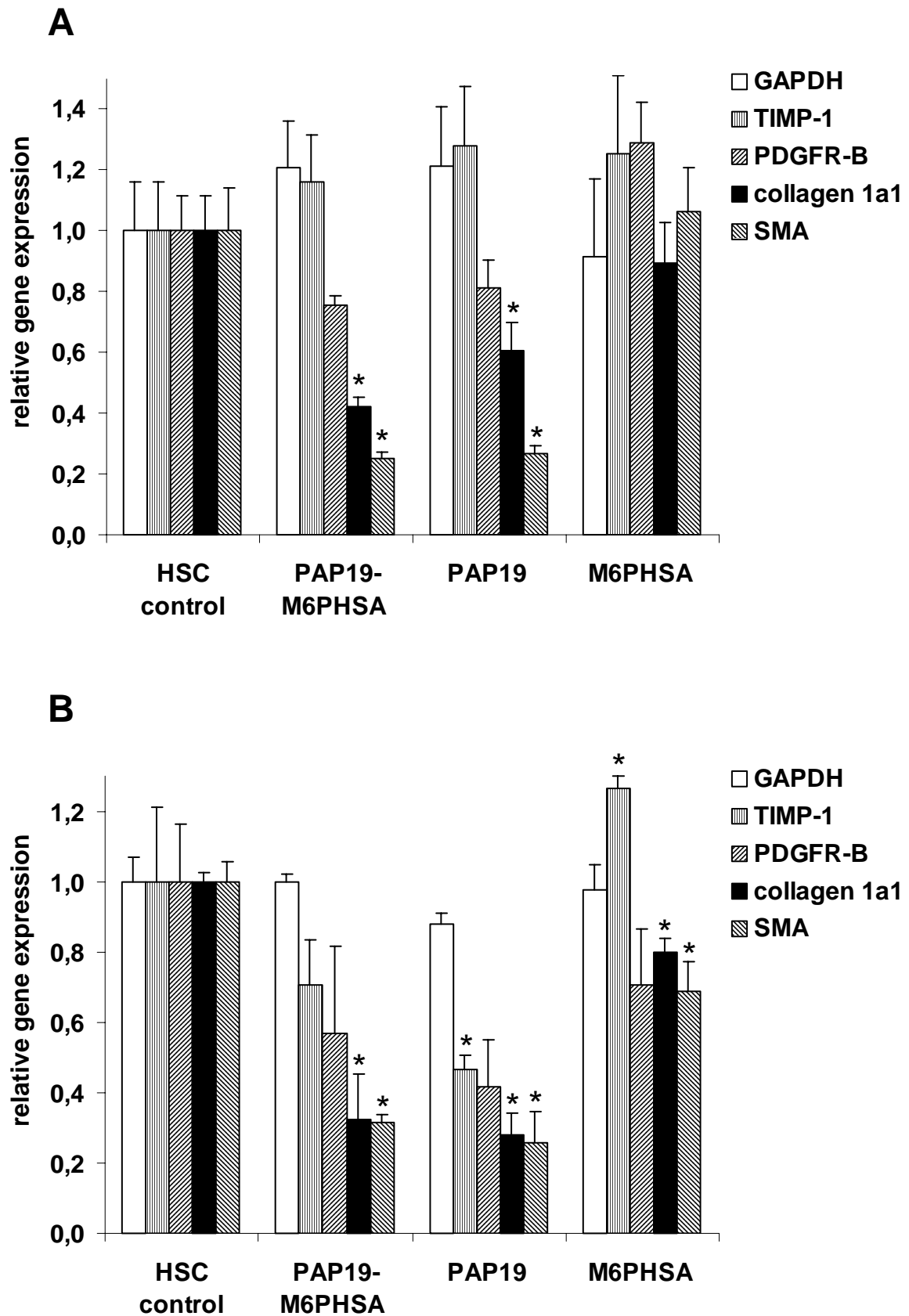


Figure 5

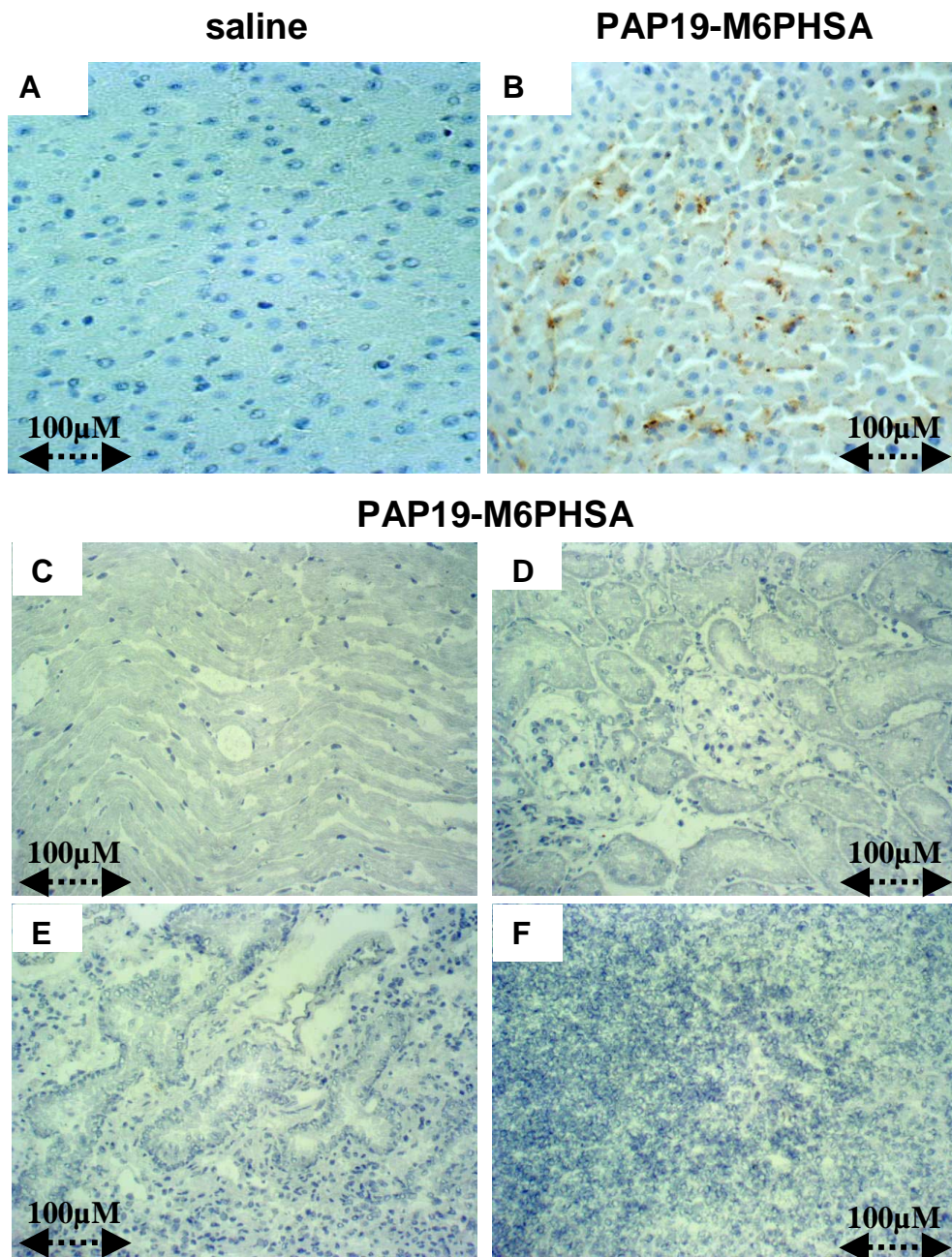


Figure 6

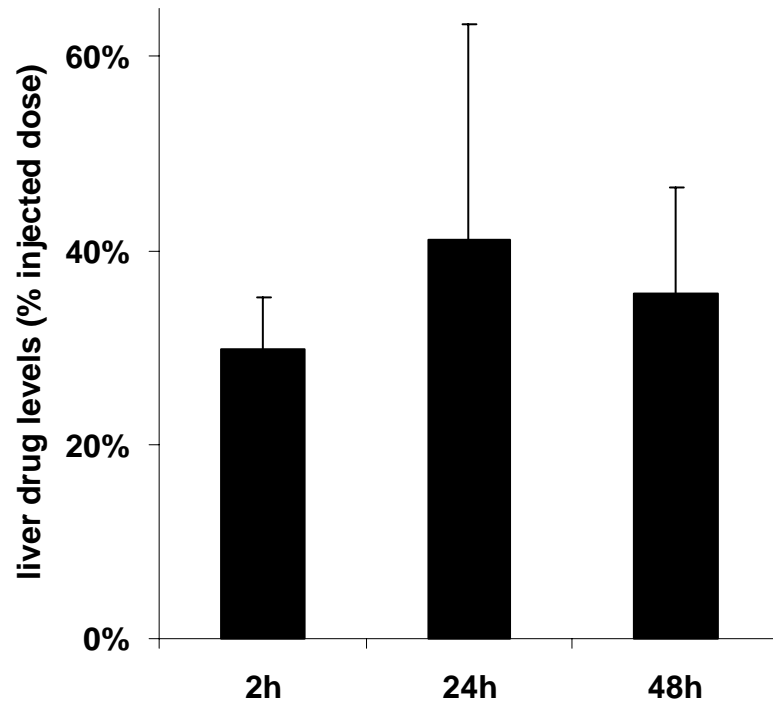


Figure 7

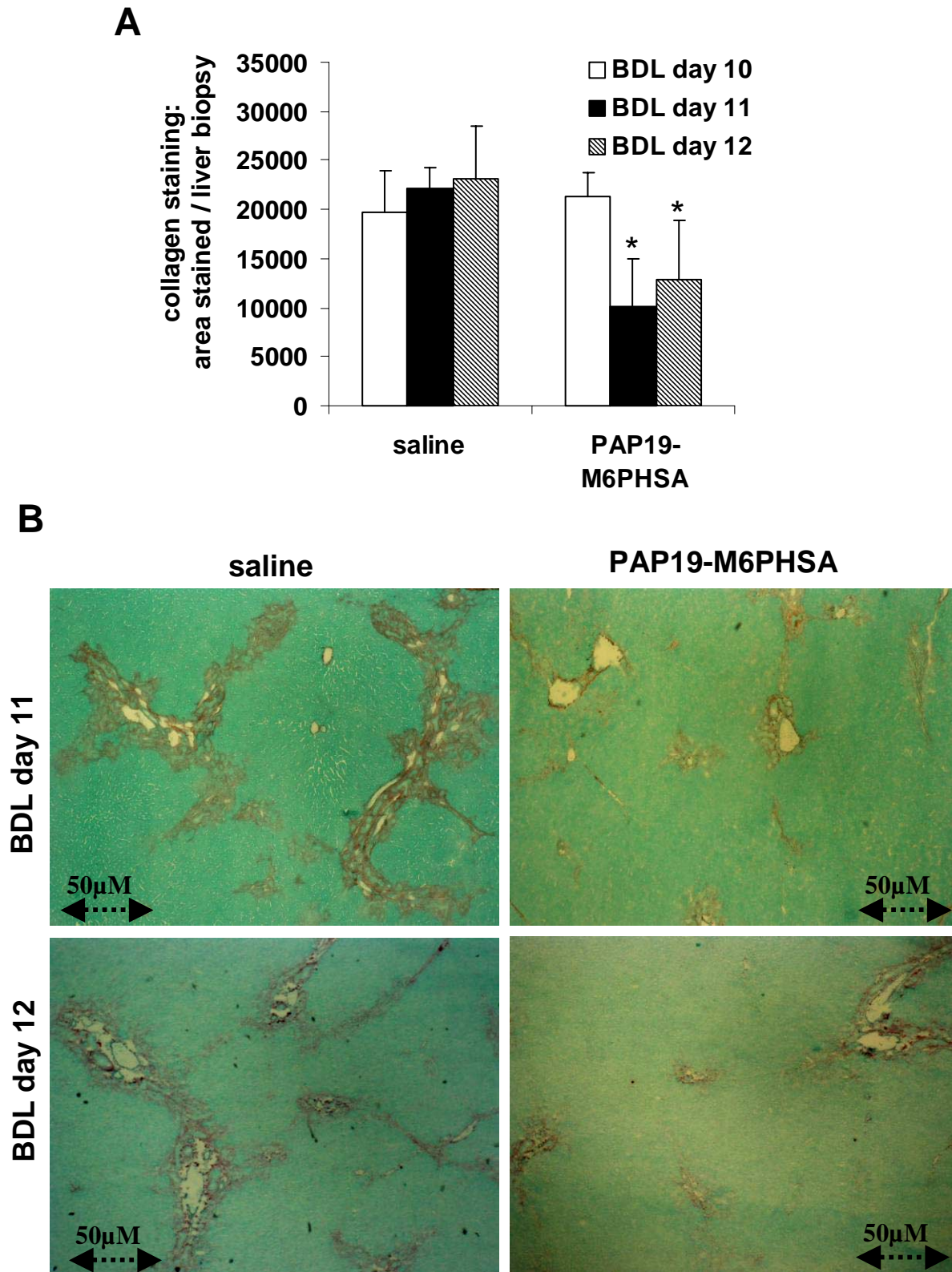


Figure 8

